PNAS
www.pnas.org

Supplementary Information for

How internal cavities destabilize a protein

Mengjun Xue, Takuro Wakamoto, Camilla Kejlberg, Yuichi Yoshimura, Tania Aaquist Nielsen, Michael Wulff Risør, Kristian Wejse Sanggaard, Ryo Kitahara, Frans A.A. Mulder

Corresponding authors: Ryo Kitahara and Frans A.A. Mulder
E-mail: ryo@ph.ritsumei.ac.jp and fmulder@chem.au.dk

This PDF file includes:

Materials and Methods
Figures S1 to S12
Tables S1 to S5
SI References

www.pnas.org/cgi/doi/10.1073/pnas.1911181116

Materials and Methods

Protein sample preparation. The L99A T4L mutant was based on a cysteine-free background T4 lysozyme (C54T/C97A; WT*) and expressed in M9 media supplemented with 1g/L $^{15}NH_4Cl$ and 3g/L D-glucose. Purification of T4L was carried out as previously described (1). The ^{15}N-labeled L99A T4L samples were prepared at 0.4 mM in 50 mM phosphate buffer and 25 mM NaCl at pH 5.5.

Native state hydrogen exchange. The protein sample was buffer exchanged into 50 mM phosphate/D_2O buffer, 25 mM NaCl (pH* 5.5, meter reading) using a 10 kDa MWCO Amicon centrifugal filter (Merck Millipore Ltd). The protein sample was transferred to a ceramic pressure-resistant NMR cell (Daedalus Innovations, PA, USA) and a series of ^{1}H-^{15}N heteronuclear single quantum coherence (HSQC) spectra were measured at 24 ^{o}C on a 600 MHz spectrometer (Bruker BioSpin Co. AVANCE) under constant hydrostatic pressures of 1 bar, 500 bar, 1000 bar, 1500 bar, 2000 bar, and 2500 bar. Spectral analyses were performed using Topspin3.1 and Bruker dynamics center software. Each HSQC spectrum was recorded with 1024 complex data points in the ^{1}H dimension and 80 complex data points in the ^{15}N dimension using 40 scans per increment. Assignments were adapted by tracking pressure-dependence of chemical shifts.

Considerations for hydrogen exchange at high pressure. Hydrogen exchange at atmospheric pressure virtually guarantees the EX2 limit under the solution conditions used here (pH* 5.5, 24 °C) (2). Validity of the EX2 limit at high pressures requires confirmation. The validation of the EX2 implies that k_{ex} increases tenfold with every unit of pH. We performed such a test at 2000 bar. Residues for which the EX2 condition applied were identified by slopes of unity in plots of the logarithms of hydrogen exchange rates versus pH (data obtained at pH* 5.50 and 5.71). Slopes < 0.7 were obtained for residues 24, 25, 52, and 62 and this data was excluded from further analysis.

The amide exchange rates, k_{ex}, were obtained by fitting the peak intensities as a function of time to a single exponential decay equation. In instances where an initial increase in intensity was observed we followed the published analysis protocol (3).

In the high-pressure experiments, pressure should be taken into account in the calculations of k_{int} (4, 5), in addition to temperature and pH. Pressure effects on the sum of the acid, base, and water hydrogen exchange rate constants k_{int} can be calculated from the activation volumes of acid-catalyzed, base-catalyzed, and un-catalyzed HX reactions ($\Delta V^{\neq}_{(H+)}$ = +1.7 mL/mol, $\Delta V^{\neq}_{(OH-)}$ = +11.0 mL/mol, $\Delta V^{\neq}_{(H2O)}$ = −9.0 mL/mol) based on equation 1 and from pressure dependence of the ionization constant of water K_W (i.e., $\Delta V^{\neq}_{(KW)}$ = −22.1 mL/mol) based on equation 2 (4, 6). The ionization state of acidic side chains was estimated by using side chain -COOH pK_a of amino acid residues Glu and Asp correcting for temperature and pressure effect (4). The ionization state of basic side chain was estimated by using side chain imidazole pK_a of amino acid residue His correcting only for temperature effect, and as the pK_a of side chain of histidine is independent of pressure (7).

$$k(p) = k_0(p_0)exp\left(-\frac{p-p_0}{RT}\Delta V^{\neq}\right) \qquad (1)$$

$$pK_W(T,p) - pK_W(T,p_0) = \frac{p\Delta V^{\neq}}{2.303RT(1+bp)} \qquad (2)$$

The effect of pressure on the pK_a and pH* of phosphate buffer was corrected (8). The predicted k_{int} values at 1 bar, 500 bar, 1000 bar, 1500 bar, 2000 bar and 2500 bar are given in Table S4. The results indicate that high pressure moderately reduces k_{int}.

^{15}N relaxation dispersion experiments. ^{15}N-Carr-Purcell-Meiboom-Gill (CPMG) NMR relaxation dispersion data were measured on a 1 mM ^{15}N labeled L99A T4L sample at 25 ^{o}C under 6 different pressures (1 bar, 200 bar, 500 bar, 700 bar, 1000 bar, and 1500 bar) using AVANCE 500 MHz and 700 MHz spectrometers (Bruker BioSpin). ^{15}N relaxation dispersion with a constant ^{15}N relaxation period of 40

ms were obtained at different CPMG field strengths (ν_{cpmg}=100 Hz (2 times), 200 Hz (2 times), 300 Hz, 400 Hz, 600 Hz (2 times), 800 Hz (2 times), and 1000 Hz). Spectral analyses were performed using Topspin3.1 and Bruker dynamics center software.

Analysis of pressure-dependent relaxation dispersion data. As access to the excited state of L99A is a global two-site exchange process (9–11) all data were modelled using the Richard-Carver equation (12) given below. At first instance the chemical shift differences were fit individually for each residue (residues L7, K19, H31, E64, K65, M120, and S136), as seen in Table S5. As these values agreed well with those determined at ambient pressure, but also displayed some variation as a consequence of the lower sensitivity attainable with the pressure cell, the chemical shift difference was subsequently fitted to a single value for all pressures for each residue. Such group fitting has previously been shown to greatly improve obtaining stable solutions for the populations and exchange rates that are needed for accurate determination of thermodynamic and kinetic parameters (9).

To extract the exchange rate (k_{ex}) and population of the excited state (p_E) (Table S3) of L99A T4L at each pressure, we performed a global fit of the NMR relaxation dispersion data for residues L7, K19, H31, E64, K65, M120, and S136 at each pressure (Figs. S7-S12) to a two-site exchange model according to the Richard-Carver equation (12), the chemical shift differences between native state and excited state were kept constant for each residue during global fitting (10). Global fitting was performed with in-house written MATLAB scripts.

$$A \Leftrightarrow B$$

$$R_2^{eff} = R_2^0 + \frac{k_{ex}}{2} - \nu_{cpmg} \cosh^{-1}\left[D_+ \cosh(\eta_+) - D_- \cos(\eta_-)\right]$$

Where

$$D_\pm = \frac{1}{2}\left[\pm 1 + \frac{\psi + 2\delta\omega^2}{\left(\psi^2 + \xi^2\right)^{0.5}}\right]$$

$$\eta_\pm = \frac{\left[\pm\psi + \left(\psi^2 + \xi^2\right)^{0.5}\right]^{0.5}}{2\sqrt{2}\nu_{cpmg}}$$

$$\psi = k_{ex}^2 - \delta\omega^2$$

$$\xi = -2\delta\omega\left(p_a k_{ex} - p_b k_{ex}\right)$$

ν_{cpmg} = 1 / (4τ) and 2τ is the time between the centers of two successive 180° pulses. Equal intrinsic transverse relaxation rates in the ground and excited states were assumed.

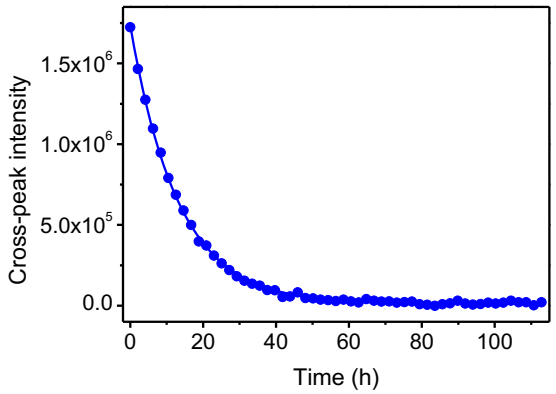

Fig. S1. Typical proton–deuterium exchange curve. Data shown is for the backbone amide hydrogen of Lys16 at 2000 bar.

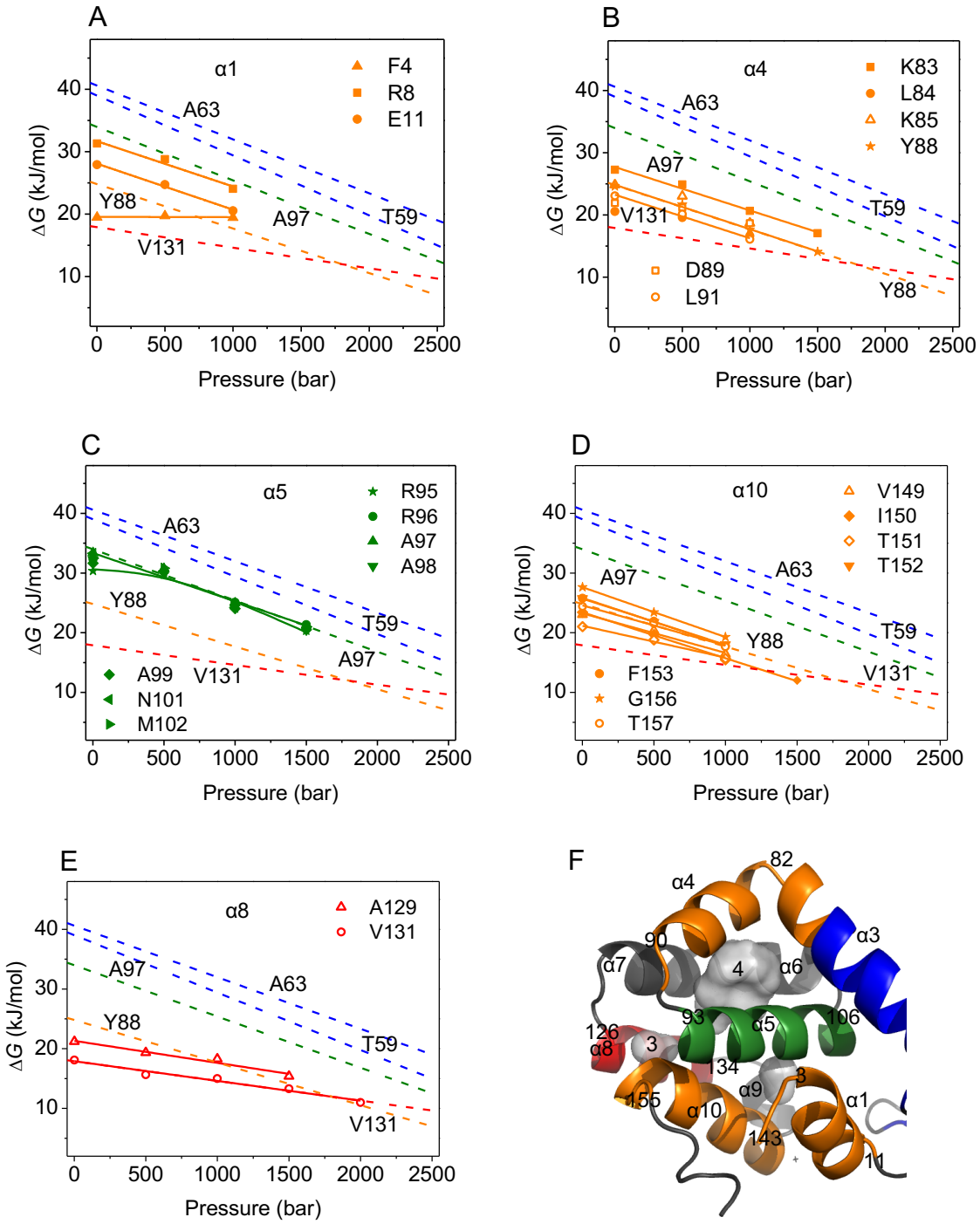

Fig. S2. Native-state HX isotherms for residues in selected helices in the CTD of L99A T4L. Pressure-dependent stabilities for residues in (A) α-helix 1, (B) α-helix 4, (C) α-helix 5, (D) α-helix 10, and (E) α-helix 8. Symbols indicate experimentally determined stabilities, and lines are fits to Equation (1) and (2); (F) Positions of the amide hydrogens detected in panels A–C illustrated on the crystal structure of L99A T4L. Cavities 3 and 4 are shown as grey space-filling models.

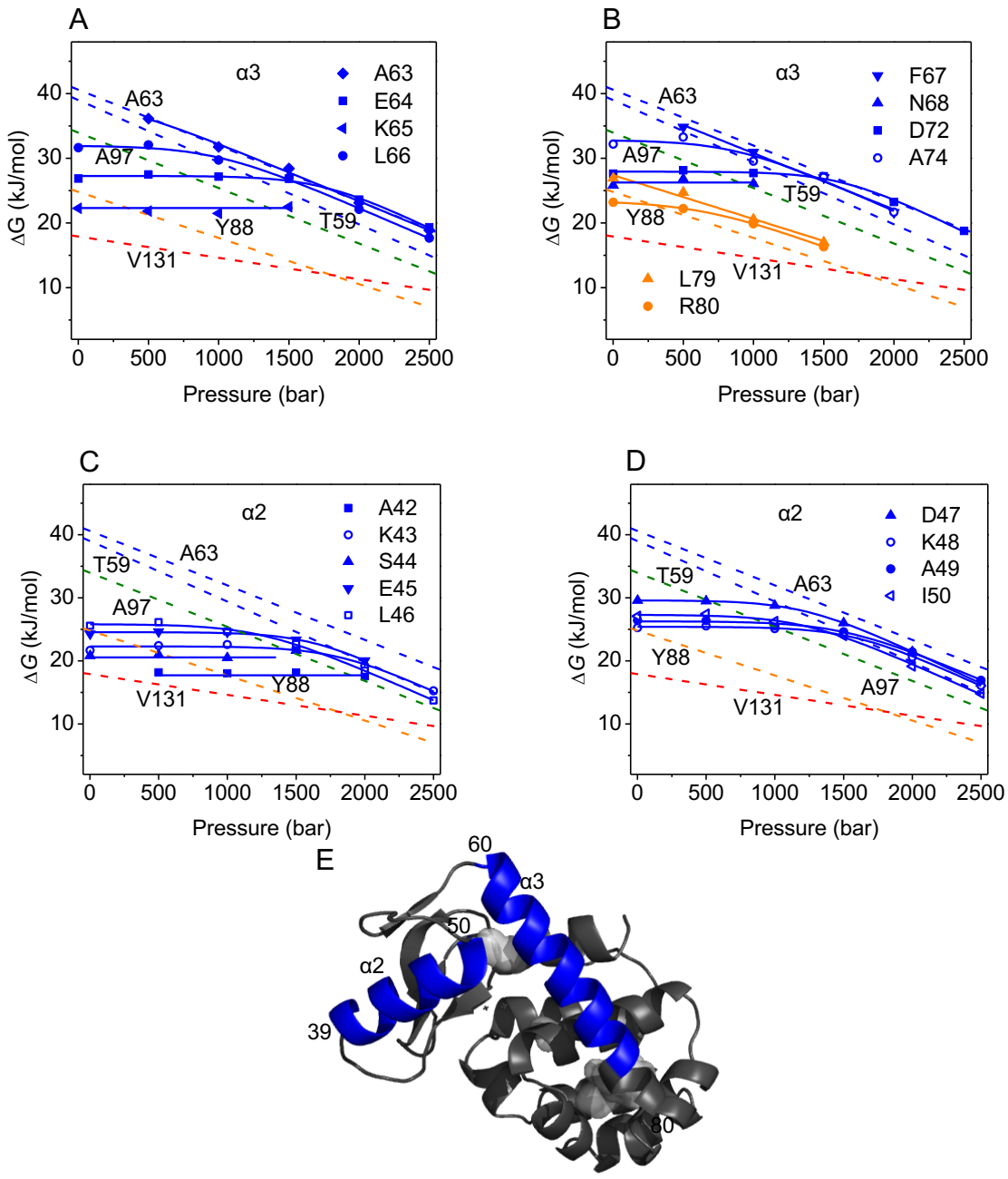

Fig. S3. Native-state HX isotherms for residues in helices of the NTD of L99A T4L. Pressure-dependent stabilities for residues in (A) and (B) α-helix 3, (C) and (D) α-helix 2. Symbols indicate experimentally determined stabilities, and lines are fits to Equations (1) and (2). (E) Positions of the amide hydrogens detected in panels A–D illustrated on the crystal structure of L99A T4L. Leu79 and Arg80 at the C terminus of α-helix 3 are categorized as part of the CTD.

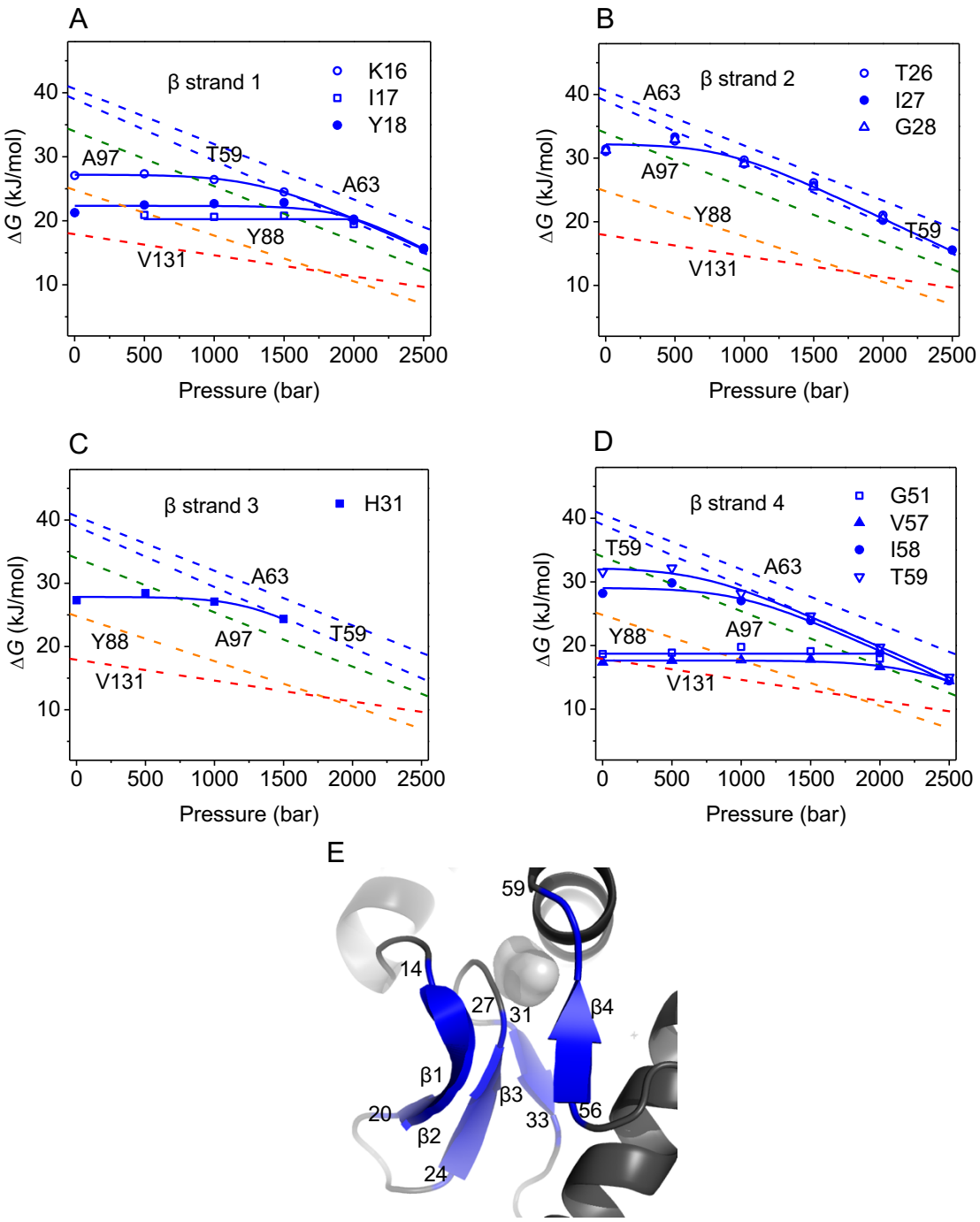

Fig. S4. Native-state HX isotherms for residues in β strands in the NTD of L99A T4L. Symbols indicate experimentally determined stabilities (A–D), and lines are fits to Equations (1) and (2). (E) Positions of the amide hydrogens detected in panels A–D illustrated on the crystal structure of L99A T4L.

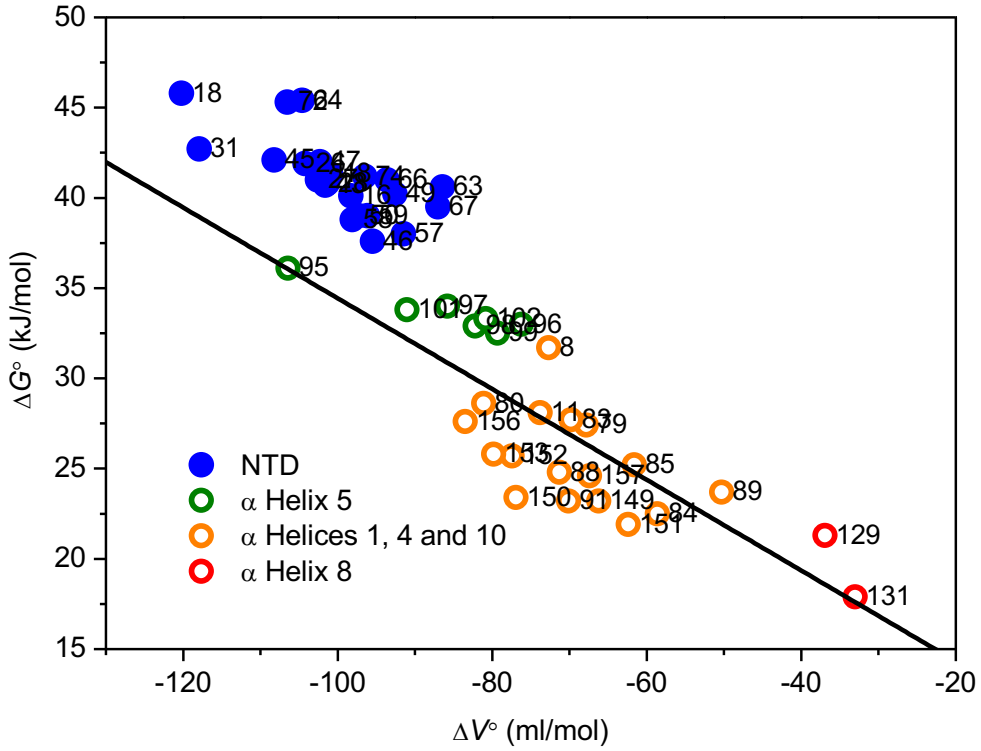

Fig. S5. Correlation of residue-specific ΔG° and ΔV° defines a broad of stabilities from which the cost of cavity formation can be determined. Data for the NTD (blue) lies on a parallel line, also reporting on the cost of cavity formation in the CTD, but appears offset by 5 kJ/mol, in agreement with the greater stability of the NTD for L99A.

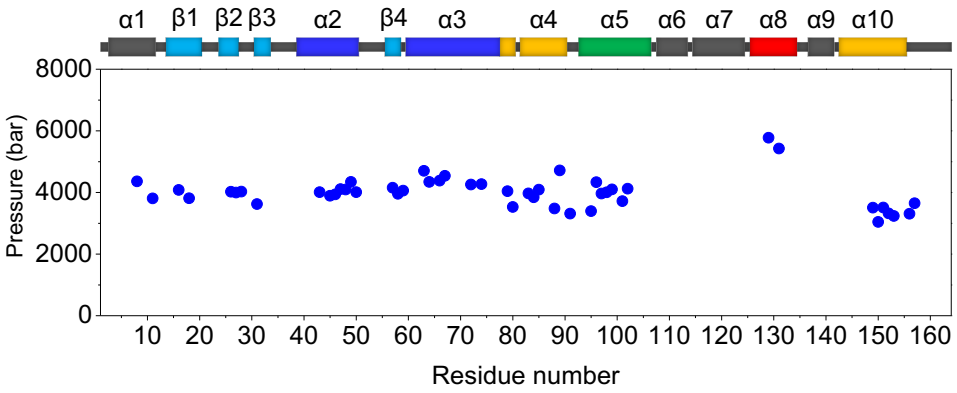

Fig. S6. Unfolding mid-point pressure p (at Δ*G*=0) of L99A T4L based on pressure dependent hydrogen exchange experiments. For A129 and V131, small values for Δ*G*º and Δ*V*º precluded the observation of the merging to global unfolding isotherms at high pressure (see Fig. 2C), causing their extrapolation to be unreliable.

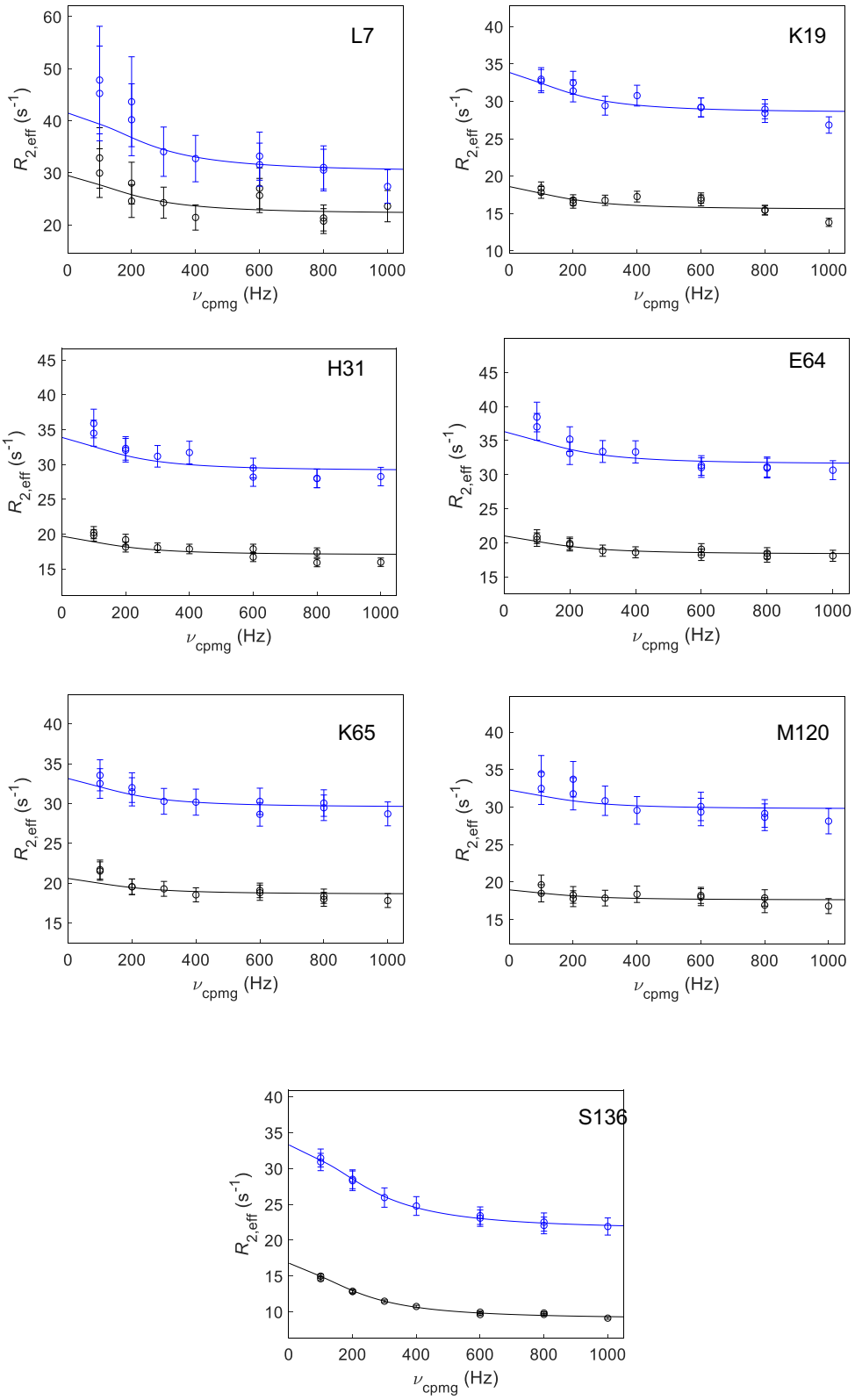

Fig. S7. ^{15}N CPMG relaxation dispersion profiles recorded at 1 bar with 500 MHz (black) and 700 MHz (blue) spectrometers for the selected residues of L99A T4L.

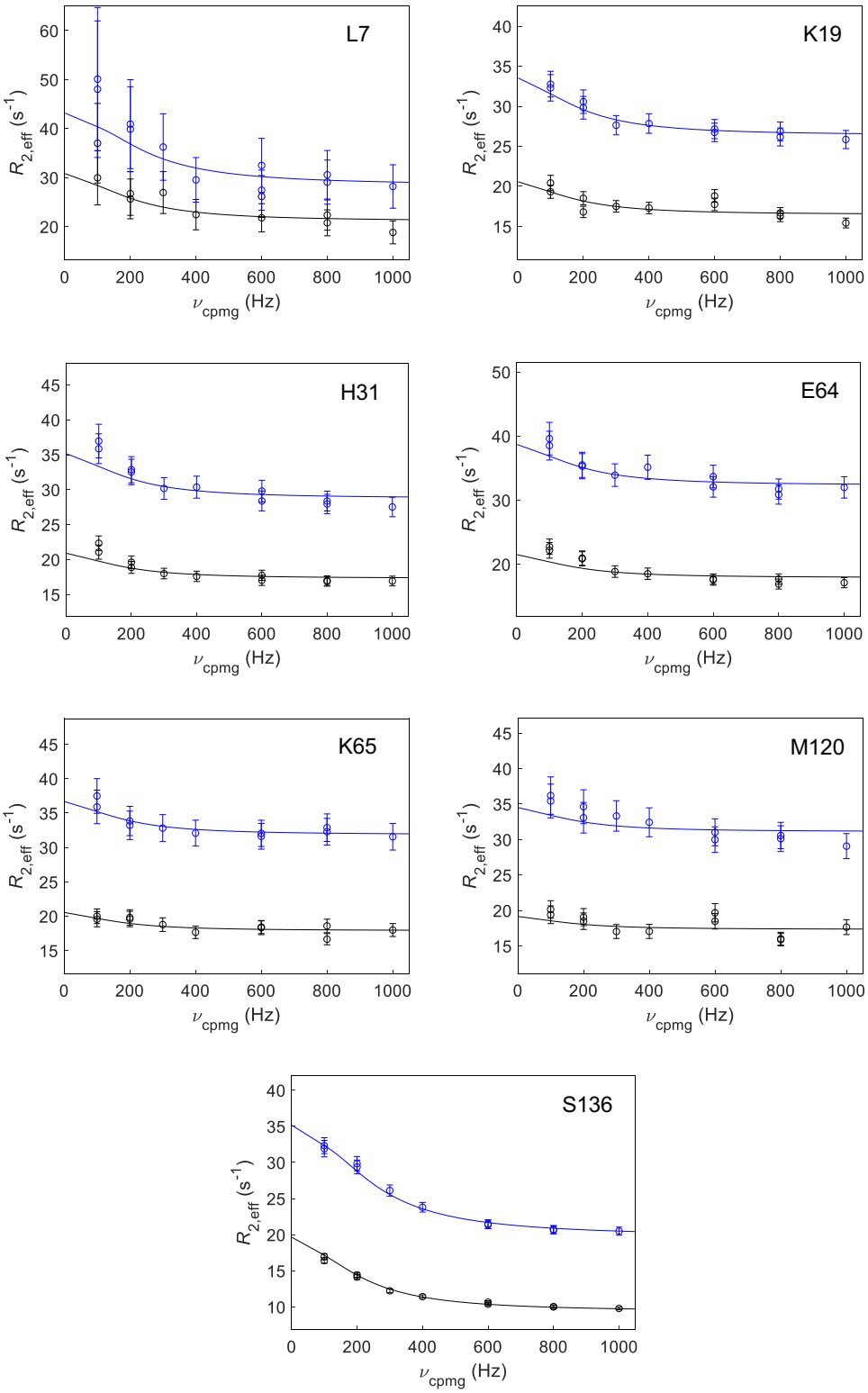

Fig. S8. ^{15}N CPMG relaxation dispersion profiles recorded at 200 bar with 500 MHz (black) and 700 MHz (blue) spectrometers for the selected residues of L99A T4L.

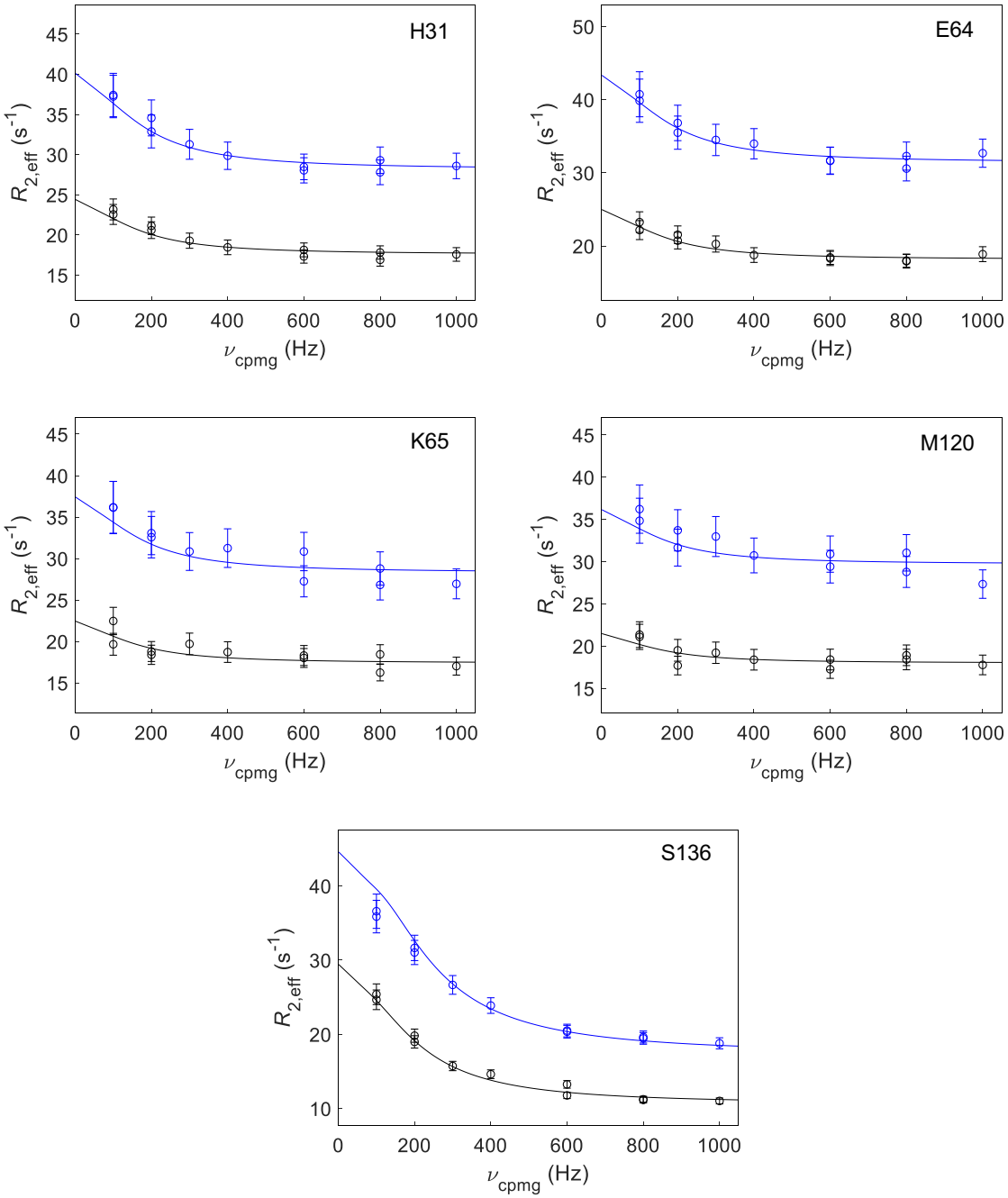

Fig. S9. ^{15}N CPMG relaxation dispersion profiles recorded at 500 bar with 500 MHz (black) and 700 MHz (blue) spectrometers for the selected residues of L99A T4L.

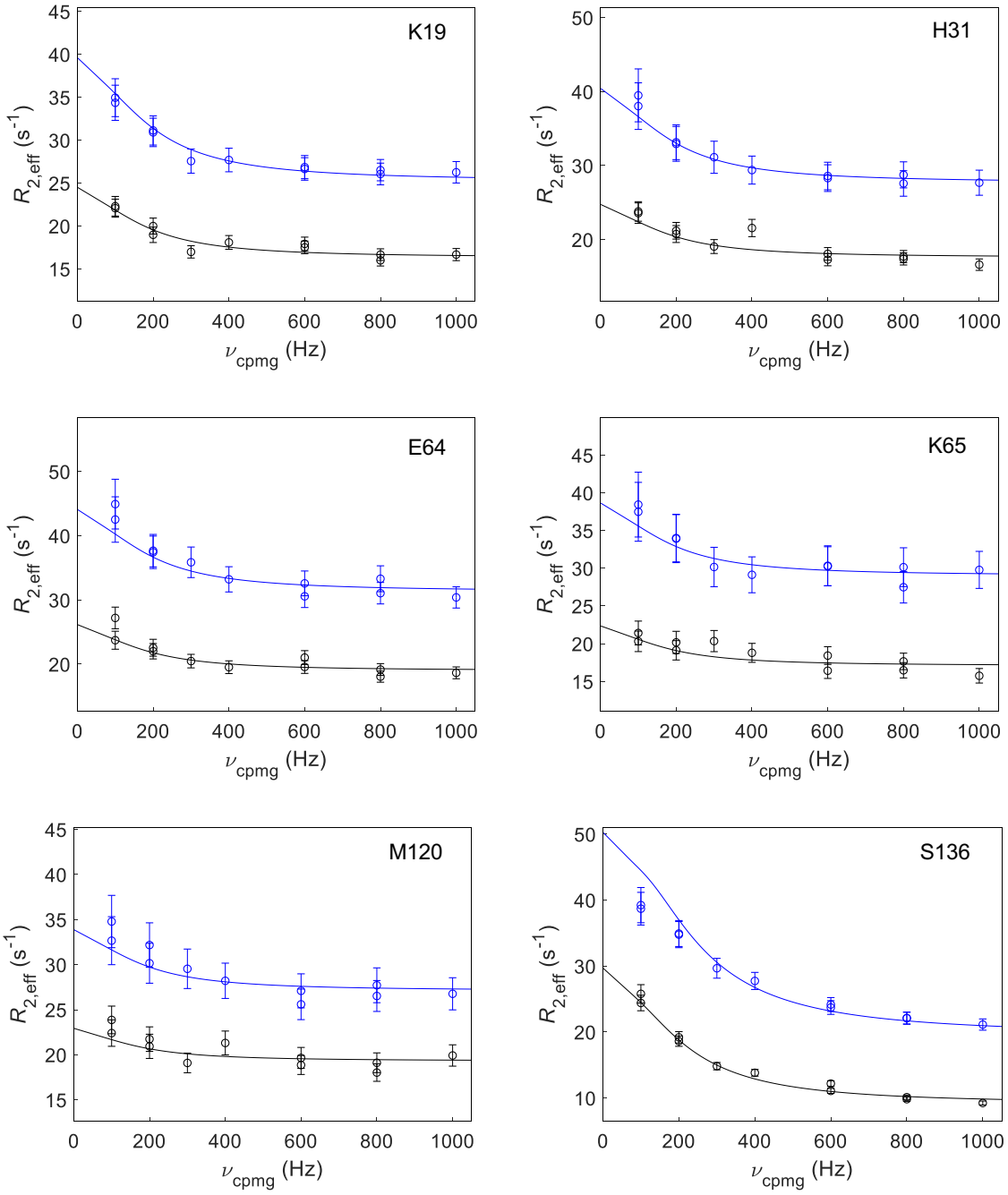

Fig. S10. ^{15}N CPMG relaxation dispersion profiles recorded at 700 bar with 500 MHz (black) and 700 MHz (blue) spectrometers for the selected residues of L99A T4L.

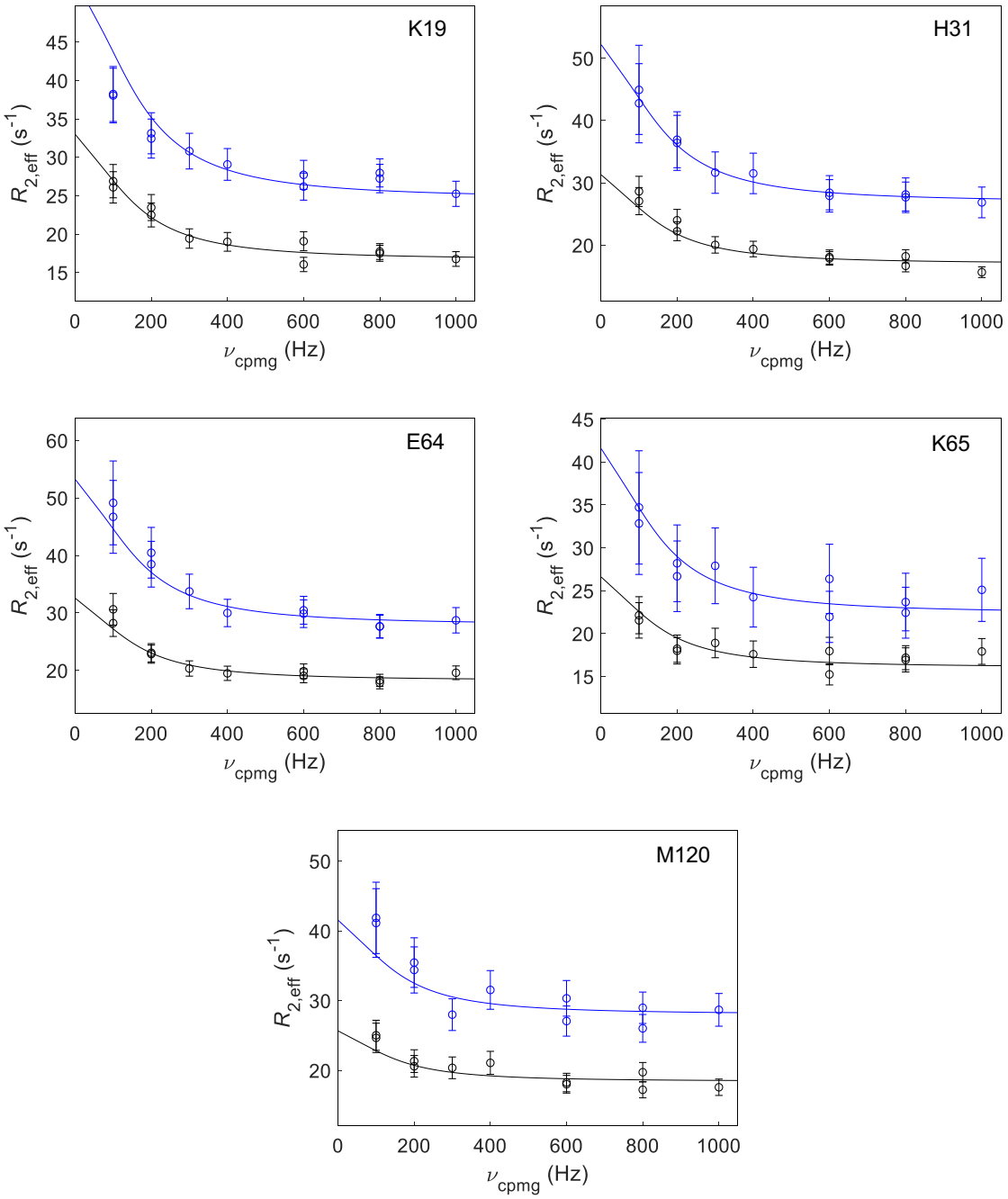

Fig. S11. ^{15}N CPMG relaxation dispersion profiles recorded at 1000 bar with 500 MHz (black) and 700 MHz (blue) spectrometers for the selected residues of L99A T4L.

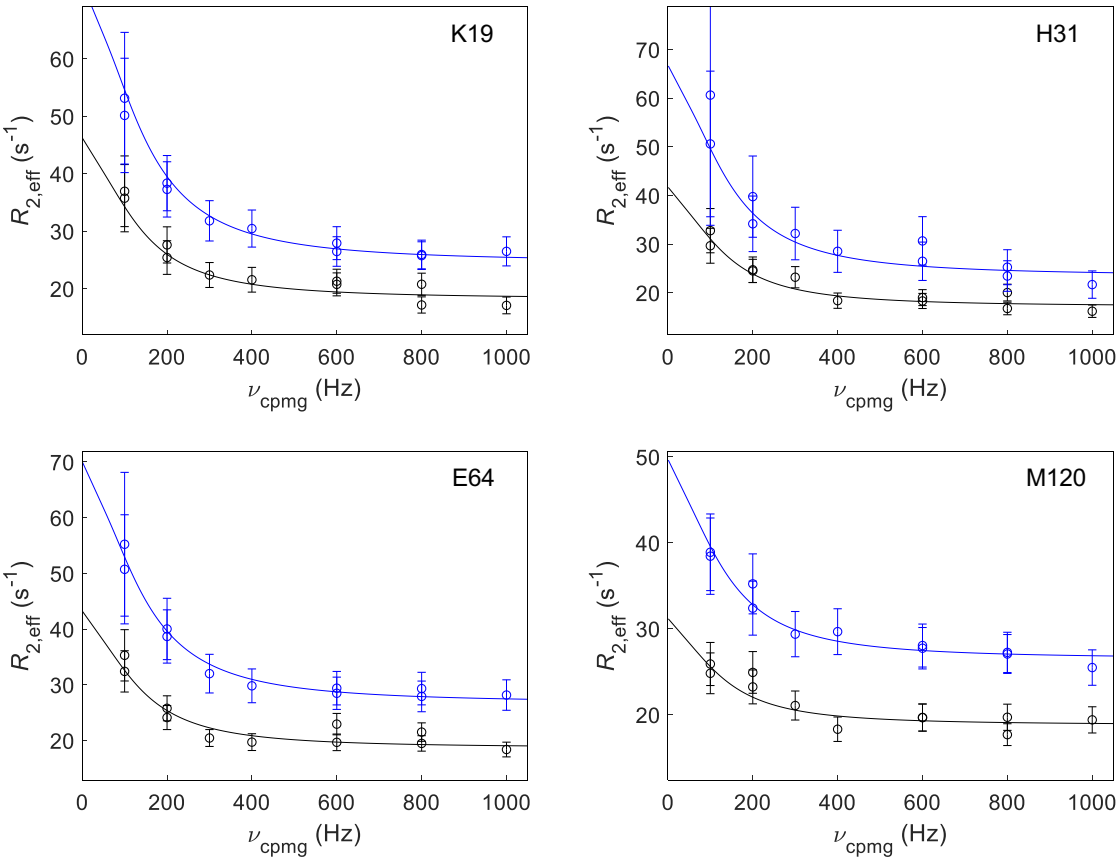

Fig. S12. ^{15}N CPMG relaxation dispersion profiles recorded at 1500 bar with 500 MHz (black) and 700 MHz (blue) spectrometers for the selected residues of L99A T4L.

Table S1. Calculated ΔV^o and ΔG^o for structural elements in L99A T4L.

Element	ΔG^o (kJ/mol)	ΔV^o (ml/mol)
α1 (4 – 11)	30±3	-73±1
α2 (42 – 50)	40±2	-100±5
β strands (16 – 33 / 51 – 59)	41±2	-103±10
α3 (63 – 74)	42±3	-96±9
α4 (79–80, 83 – 91)	25±2	-66±9
α5 (95 – 102)	34±1	-86±10
α8 (129 – 131)	20±2	-35±3
α10 (149 – 157)	25±2	-73±8

Table S2. Calculated ΔG^o and ΔV^o for amino-acid residues in L99A T4L.

Residue	ΔG^o(kJ/mol)	ΔV^o (ml/mol)	No. pressures used in fit	Model
R8	31.7	-72.7	3	2-parameters
E11	28.1	-73.8	3	2-parameters
K16	40.1	-98.3	6	3-parameters
Y18	45.8	-120.2	6	3-parameters
T26	41.9	-104.2	5	3-parameters
I27	41	-102.6	6	3-parameters
G28	40.8	-101.3	5	3-parameters
H31	42.7	-117.9	4	3-parameters
K43	40.7	-101.6	6	3-parameters
E45	42.1	-108.2	6	3-parameters
L46	37.6	-95.5	6	3-parameters
D47	42	-102.3	6	3-parameters
K48	41.3	-100.9	6	3-parameters
A49	40.2	-92.6	6	3-parameters
I50	39	-97.3	6	3-parameters
V57	38	-91.5	6	3-parameters
I58	38.8	-98.1	6	3-parameters
T59	39	-96.1	6	3-parameters
A63	40.6	-86.4	5	2-parameters
E64	45.4	-104.6	6	3-parameters
L66	41	-93.6	6	3-parameters
F67	39.5	-87	4	2-parameters
D72	45.3	-106.5	6	3-parameters
A74	41.2	-96.5	5	3-parameters
L79	27.4	-67.8	5	2-parameters
R80	28.6	-81.1	4	3-parameters
K83	27.7	-69.8	4	2-parameters
L84	22.5	-58.6	3	2-parameters[a]
K85	25.2	-61.6	3	2-parameters
Y88	24.8	-71.3	4	2-parameters
D89	23.7	-50.3	3	2-parameters [a]
L91	23.2	-70.1	3	2-parameters
R95	36.1	-106.4	4	3-parameters
R96	33	-76.2	4	2-parameters
A97	34	-85.8	4	2-parameters
A98	32.9	-82.2	4	2-parameters

A99	32.5	-79.3	4	2-parameters
N101	33.8	-91	3	2-parameters
M102	33.3	-80.8	4	2-parameters
A129	21.3	-36.9	4	2-parameters
V131	17.9	-33	5	2-parameters
V149	23.2	-66.2	3	2-parameters
I150	23.4	-76.9	4	2-parameters
T151	21.9	-62.4	3	2-parameters [a]
T152	25.7	-77.4	3	2-parameters
F153	25.8	-79.8	3	2-parameters
G156	27.6	-83.5	3	2-parameters
T157	24.6	-67.4	3	2-parameters

[a] Analyzed using data points at 500 and 1000 bar only.

Table S3. Values obtained from the global fit of NMR dispersion measurement for L99A T4L at 1 bar, 200 bar, 500 bar, 700 bar, 1000 bar, and 1500 bar. p_E is the population of excited state.

Pressure (bar)	k_{ex} (s^{-1})	p_E (%)
1	1190±129	2.1±0.1
200	1129±114	2.7±0.1
500	993±138	4.8±0.2
700	1093±139	5.4±0.2
1000	938±187	10.1±0.8
1500	808±174	16.0±1.5

Table S4. Predicted k_{int} for amino-acid residues of unstructured peptide of L99A T4L in pH* 5.5 phosphate buffer at 24 °C under 1 bar, 500 bar, 1000 bar, 1500 bar, 2000 bar, and 2500 bar.

Residue number	k_{int} at 1 bar (s^{-1})	k_{int} at 500 bar (s^{-1})	k_{int} at 1000 bar (s^{-1})	k_{int} at 1500 bar (s^{-1})	k_{int} at 2000 bar (s^{-1})	k_{int} at 2500 bar (s^{-1})
N2	31.5	29.5	27.3	25.1	22.7	20.5
I3	0.074	0.069	0.064	0.059	0.053	0.048
F4	0.065	0.061	0.056	0.052	0.047	0.042
E5	0.188	0.177	0.165	0.152	0.138	0.125
M6	0.159	0.151	0.141	0.13	0.119	0.108
L7	0.065	0.061	0.056	0.052	0.047	0.042
R8	0.139	0.131	0.121	0.111	0.101	0.091
I9	0.059	0.055	0.051	0.047	0.042	0.038
D10	0.154	0.145	0.135	0.124	0.113	0.102
E11	0.125	0.119	0.111	0.103	0.094	0.086
G12	0.301	0.285	0.266	0.246	0.224	0.204
L13	0.074	0.07	0.065	0.059	0.054	0.049
R14	0.139	0.131	0.121	0.111	0.101	0.091
L15	0.083	0.078	0.072	0.067	0.06	0.055
K16	0.107	0.1	0.093	0.085	0.077	0.07
I17	0.047	0.044	0.04	0.037	0.034	0.03
Y18	0.06	0.056	0.052	0.048	0.043	0.039
K19	0.194	0.182	0.168	0.155	0.14	0.127
D20	0.344	0.324	0.302	0.278	0.253	0.229
T21	0.125	0.118	0.11	0.102	0.093	0.084
E22	0.258	0.243	0.226	0.209	0.19	0.172
G23	0.301	0.285	0.266	0.246	0.224	0.204
Y24	0.151	0.141	0.131	0.12	0.109	0.098
Y25	0.114	0.107	0.099	0.091	0.082	0.075
T26	0.183	0.171	0.159	0.146	0.132	0.119
I27	0.056	0.052	0.049	0.045	0.04	0.037
G28	0.206	0.194	0.179	0.165	0.149	0.135
I29	0.052	0.049	0.045	0.042	0.038	0.034
G30	0.206	0.194	0.179	0.165	0.149	0.135
H31	1.665	1.565	1.454	1.341	1.214	1.1
L32	0.322	0.302	0.281	0.259	0.234	0.212
L33	0.031	0.029	0.027	0.025	0.022	0.02
T34	0.1	0.094	0.087	0.08	0.072	0.066
K35	0.274	0.257	0.238	0.219	0.198	0.179

S36	0.586	0.549	0.509	0.468	0.423	0.383
P37						
S38	0.256	0.24	0.222	0.204	0.185	0.167
L39	0.1	0.094	0.087	0.08	0.072	0.065
N40	0.361	0.339	0.314	0.289	0.261	0.236
A41	0.396	0.371	0.344	0.317	0.286	0.259
A42	0.19	0.178	0.165	0.152	0.137	0.124
K43	0.173	0.162	0.15	0.138	0.125	0.113
S44	0.586	0.549	0.509	0.468	0.423	0.383
E45	0.325	0.306	0.284	0.263	0.238	0.216
L46	0.043	0.041	0.038	0.035	0.032	0.029
D47	0.161	0.152	0.141	0.13	0.118	0.107
K48	0.133	0.126	0.117	0.108	0.099	0.09
A49	0.25	0.234	0.217	0.2	0.18	0.163
I50	0.035	0.033	0.031	0.028	0.025	0.023
G51	0.206	0.194	0.179	0.165	0.149	0.135
R52	0.334	0.314	0.29	0.267	0.242	0.219
N53	0.972	0.911	0.844	0.777	0.702	0.635
T54	0.34	0.319	0.295	0.272	0.246	0.222
N55	0.928	0.87	0.806	0.742	0.67	0.606
G56	0.733	0.687	0.636	0.586	0.529	0.479
V57	0.056	0.052	0.048	0.045	0.04	0.036
I58	0.026	0.024	0.022	0.02	0.018	0.017
T59	0.096	0.09	0.083	0.077	0.069	0.063
K60	0.274	0.257	0.238	0.219	0.198	0.179
D61	0.344	0.324	0.302	0.278	0.253	0.229
E62	0.125	0.119	0.111	0.103	0.094	0.086
A63	0.163	0.154	0.144	0.133	0.121	0.11
E64	0.163	0.153	0.143	0.132	0.12	0.108
K65	0.148	0.14	0.131	0.121	0.11	0.1
L66	0.066	0.062	0.058	0.053	0.048	0.043
F67	0.068	0.064	0.059	0.054	0.049	0.044
N68	0.677	0.635	0.588	0.541	0.489	0.442
Q69	0.455	0.426	0.395	0.363	0.328	0.297
D70	0.414	0.39	0.363	0.335	0.304	0.276
V71	0.029	0.027	0.026	0.024	0.021	0.02
D72	0.189	0.178	0.166	0.153	0.139	0.126
A73	0.146	0.138	0.128	0.119	0.108	0.098
A74	0.19	0.178	0.165	0.152	0.137	0.124
V75	0.038	0.035	0.033	0.03	0.027	0.025
R76	0.164	0.154	0.142	0.131	0.118	0.107

G77	0.582	0.546	0.505	0.465	0.42	0.38
I78	0.052	0.049	0.045	0.042	0.038	0.034
L79	0.03	0.028	0.026	0.024	0.021	0.019
R80	0.139	0.131	0.121	0.111	0.101	0.091
N81	0.972	0.911	0.844	0.777	0.702	0.635
A82	0.396	0.371	0.344	0.317	0.286	0.259
K83	0.173	0.162	0.15	0.138	0.125	0.113
L84	0.066	0.062	0.058	0.053	0.048	0.043
K85	0.107	0.1	0.093	0.085	0.077	0.07
P86						
V87	0.022	0.02	0.019	0.017	0.016	0.014
Y88	0.074	0.069	0.064	0.059	0.053	0.048
D89	0.293	0.276	0.257	0.237	0.215	0.195
S90	0.342	0.323	0.301	0.279	0.253	0.23
L91	0.1	0.094	0.087	0.08	0.072	0.065
D92	0.161	0.152	0.141	0.13	0.118	0.107
A93	0.146	0.138	0.128	0.119	0.108	0.098
V94	0.038	0.035	0.033	0.03	0.027	0.025
R95	0.164	0.154	0.142	0.131	0.118	0.107
R96	0.375	0.352	0.326	0.3	0.271	0.245
A97	0.315	0.295	0.273	0.251	0.227	0.205
A98	0.19	0.178	0.165	0.152	0.137	0.124
A99	0.19	0.178	0.165	0.152	0.137	0.124
I100	0.035	0.033	0.031	0.028	0.025	0.023
N101	0.345	0.323	0.3	0.276	0.249	0.225
M102	0.388	0.364	0.337	0.31	0.28	0.253
V103	0.048	0.045	0.042	0.039	0.035	0.032
F104	0.08	0.075	0.069	0.064	0.058	0.052
Q105	0.252	0.236	0.219	0.201	0.182	0.164
M106	0.294	0.276	0.256	0.235	0.213	0.192
G107	0.452	0.424	0.392	0.361	0.326	0.295
E108	0.241	0.227	0.211	0.195	0.177	0.16
T109	0.14	0.132	0.123	0.114	0.104	0.095
G110	0.556	0.521	0.483	0.444	0.401	0.363
V111	0.056	0.052	0.048	0.045	0.04	0.036
A112	0.137	0.129	0.119	0.11	0.099	0.09
G113	0.351	0.329	0.305	0.28	0.253	0.229
F114	0.163	0.153	0.141	0.13	0.118	0.106
T115	0.188	0.176	0.163	0.15	0.136	0.123
N116	0.928	0.87	0.806	0.742	0.67	0.606
S117	0.928	0.87	0.806	0.742	0.67	0.606

L118	0.1	0.094	0.087	0.08	0.072	0.065
R119	0.139	0.131	0.121	0.111	0.101	0.091
M120	0.308	0.289	0.268	0.246	0.223	0.201
L121	0.065	0.061	0.056	0.052	0.047	0.042
Q122	0.134	0.126	0.117	0.107	0.097	0.088
Q123	0.345	0.323	0.3	0.276	0.249	0.225
K124	0.274	0.257	0.238	0.219	0.198	0.179
R125	0.298	0.279	0.259	0.238	0.215	0.195
W126	0.122	0.115	0.106	0.098	0.088	0.08
D127	0.203	0.191	0.178	0.164	0.149	0.135
E128	0.125	0.119	0.111	0.103	0.094	0.086
A129	0.163	0.154	0.144	0.133	0.121	0.11
A130	0.19	0.178	0.165	0.152	0.137	0.124
V131	0.038	0.035	0.033	0.03	0.027	0.025
N132	0.424	0.398	0.368	0.339	0.306	0.277
L133	0.105	0.098	0.091	0.084	0.076	0.069
A134	0.117	0.11	0.101	0.093	0.084	0.076
K135	0.173	0.162	0.15	0.138	0.125	0.113
S136	0.586	0.549	0.509	0.468	0.423	0.383
R137	0.451	0.423	0.391	0.36	0.326	0.294
W138	0.122	0.115	0.106	0.098	0.088	0.08
Y139	0.079	0.074	0.069	0.063	0.057	0.052
N140	0.657	0.616	0.571	0.525	0.475	0.429
Q141	0.455	0.426	0.395	0.363	0.328	0.297
T142	0.258	0.242	0.224	0.206	0.186	0.168
P143						
N144	0.337	0.316	0.293	0.269	0.243	0.22
R145	0.472	0.443	0.41	0.378	0.341	0.309
A146	0.315	0.295	0.273	0.251	0.227	0.205
K147	0.173	0.162	0.15	0.138	0.125	0.113
R148	0.298	0.279	0.259	0.238	0.215	0.195
V149	0.062	0.059	0.054	0.05	0.045	0.041
I150	0.026	0.024	0.022	0.02	0.018	0.017
T151	0.096	0.09	0.083	0.077	0.069	0.063
T152	0.258	0.242	0.224	0.206	0.186	0.168
F153	0.174	0.164	0.152	0.14	0.126	0.114
R154	0.262	0.245	0.227	0.209	0.189	0.171
T155	0.27	0.253	0.234	0.216	0.195	0.176
G156	0.556	0.521	0.483	0.444	0.401	0.363
T157	0.241	0.226	0.209	0.192	0.174	0.157
W158	0.117	0.11	0.101	0.093	0.084	0.076

D159	0.203	0.191	0.178	0.164	0.149	0.135
A160	0.146	0.138	0.128	0.119	0.108	0.098
Y161	0.102	0.095	0.088	0.081	0.074	0.066
K162	0.194	0.182	0.168	0.155	0.14	0.127
N163	0.772	0.724	0.671	0.617	0.558	0.504
L164						

Table S5. Absolute values of ^{15}N chemical shift differences (in ppm) for L99A at various pressures for residues L7, K19, H31, E64, K65, M120, and S136 extracted by CPMG relaxation dispersion NMR spectroscopy.

	1bar	200bar	500bar	700bar	1000bar	1500bar
L7	2.6	2.8				
K19	1.4	1.4		1.8	2.2	1.9
H31	1.7	1.7	1.9	2.0	2.6	1.8
E64	1.5	1.7	1.7	2.1	2.4	1.7
K65	1.4	1.2	1.5	1.7	1.5	
M120	1.2	1.4	1.3	1.6	1.9	1.2
S136	2.1	2.2	3.3	3.7		

SI References

1. P. Vallurupalli, D. F. Hansen, P. Lundström, L. E. Kay, CPMG relaxation dispersion NMR experiments measuring glycine $^{1}H_{\alpha}$ and $^{13}C_{\alpha}$ chemical shifts in the 'invisible' excited states of proteins. *J. Biomol. NMR* **45**, 45–55 (2009).
2. Y. Bai, T. R. Sosnick, L. Mayne, S. W. Englander, Protein folding intermediates: Native-state hydrogen exchange. *Science* **269**, 192–197 (1995).
3. M. Xue, R. Kitahara, Y. Yoshimura, F. A. A. Mulder, Aberrant increase of NMR signal in hydrogen exchange experiments. Observation and explanation. *Biochem. Biophys. Res. Commun.* **478**, 1185–1188 (2016).
4. E. J. Fuentes, A. J. Wand, Local stability and dynamics of apocytochrome b_{562} examined by the dependence of hydrogen exchange on hydrostatic pressure. *Biochemistry* **37**, 9877–9883, (1998).
5. Y. Bai, J. S. Milne, L. Mayne, S. W. Englander, Primary structure effects on peptide group hydrogen exchange. *Proteins* **17**, 75–86 (1993).
6. S. A. Mabry, B.-S. Lee, T. Zheng, J. Jonas, Determination of the activation volume of the uncatalyzed hydrogen exchange reaction between N-methylacetamide and water. *J. Am. Chem. Soc.* **118**, 8887–8890 (1996).
7. J. Hauer, K. Müller, H.-D. Lüdemann, R. Jaenicke, The pressure dependence of the histidine ring protonation constant studied by ^{1}H HR-NMR. *FEBS Lett.* **135**,135–138 (1981).
8. S. K. Min, C. P. Samaranayake, S. K. Sastry, In situ measurement of reaction volume and calculation of pH of weak acid buffer solutions under high pressure. *J. Phys. Chem. B* **115**, 6564–6571 (2011).
9. F. A. A. Mulder, A. Mittermaier, B. Hon, F. W. Dahlquist, L. E. Kay, Studying excited states of proteins by NMR spectroscopy. *Nat. Struct. Biol.* **8**, 932–935, (2001).
10. G. Bouvignies, P. Vallurupalli, D. F. Hansen, B. E. Correia, O. Lange, A. Bah, R. M. Vernon, F. W. Dahlquist, D. Baker, L. E. Kay, Solution structure of a minor and transiently formed state of a T4 lysozyme mutant. *Nature* **477**, 111–114, (2011).
11. F. A. A. Mulder, B. Hon, A. Mittermaier, F. W. Dahlquist, L. E. Kay, Slow internal dynamics in proteins: Application of NMR relaxation dispersion spectroscopy to methyl groups in a cavity mutant of T4 lysozyme. *J. Am. Chem. Soc.* **124**, 1443–1451 (2002).
12. J. P. Carver, R. E. Richards, General 2-site solution for chemical exchange produced dependence of T_2 upon Carr-Purcell pulse separation. *J. Magn. Reson.* **6**, 89–105 (1972).